Original paper

Thermodynamics of the Cu, Zn, and Cu–Zn phases: zincolivenite, adamite, olivenite, ludjibaite, strashimirite, and slavkovite

Juraj MAJZLAN[1]*, Martin ŠTEVKO[2,3], Jakub PLÁŠIL[4], Jiří SEJKORA[3], Edgar DACHS[5]

[1] *Institute of Geosciences, Friedrich-Schiller University, Burgweg 11, 07749 Jena, Germany; Juraj.Majzlan@uni-jena.de*
[2] *Earth Science Institute of the Slovak Academy of Sciences, Ďumbierska 1, 974 01 Banská Bystrica, Slovakia*
[3] *Department of Mineralogy and Petrology, National Museum, Cirkusová 1740, 193 00 Praha 9, Czech Republic*
[4] *Institute of Physics of the Czech Academy of Sciences, Na Slovance 1999/2, 182 21 Praha 8, Czech Republic*
[5] *Department of Chemistry and Physics of Materials, University of Salzburg, Jakob-Haringer-Strasse 2a, 5020 Salzburg, Austria*
** Corresponding author*

Secondary minerals, especially phosphates and arsenates of copper and zinc, form a group of phases with astonishing variability in crystal structures and chemical composition. Some of these minerals are more common than others and one has to ask whether the abundance is linked to their thermodynamic stability or rather to geochemical constraints. In this work, we used calorimetric techniques to determine the thermodynamic properties of synthetic olivenite [$Cu_2(AsO_4)(OH)$], zincolivenite [$Cu_{0.95}Zn_{1.05}(AsO_4)(OH)$], adamite [$Zn_2(AsO_4)(OH)$], ludjibaite [$Cu_5(PO_4)_2(OH)_4$], natural strashimirite [$(Cu_{7.75}Zn_{0.09})_{7.84}(AsO_4)_{3.89}(SO_4)_{0.11}(OH)_{3.79}\cdot 5H_2O$], and a slavkovite sample dehydrated to the composition $Cu_{12}(AsO_4)_4(AsO_3OH)_6\cdot 14H_2O$ that is used as a proxy for slavkovite. All thermodynamic data presented are based upon the compositions given above. The enthalpies of formation (at 298.15 K and 1 bar, all in kJ·mol^{-1}) are –1401.7 ± 2.6 (adamite), –1211.6 ± 3.2 (zincolivenite), –3214.3 ± 10.7 (ludjibaite), –5374.9 ± 18.1 (strashimirite), and –12004 ± 34 (dehydrated slavkovite). Entropy was measured only for ludjibaite (389.0 ± 2.7 J·K^{-1}·mol^{-1}) and estimated for other phases. Gibbs free energies of formation (all in kJ·mol^{-1}) were calculated for ludjibaite (–2811.4 ± 10.7), strashimirite (–4477.0 ± 18.3), and dehydrated slavkovite (–9987 ± 35). The dehydrated slavkovite is the consequence of H_2O loss from the slavkovite holotype specimens during storage of the samples in air at room temperature. It is triclinic ($P\bar{1}$), with unit-cell parameters a = 6.4042(11) Å, b = 13.495 (2) Å, c = 13.574 (2) Å, α = 87.009(15)°, β = 85.564(14)°, γ = 79.678(15)°. Dehydration of slavkovite results in a collapse of the sheet structure into a framework structure and into reorganization of bonding, including protonation/deprotonation of AsO_4 groups. Constructed activity–activity phase diagrams show that the less stable phases are those which are less common in nature, such as euchroite, strashimirite, or slavkovite. Zincolivenite is stabilized with respect to the end-members olivenite and adamite by a small enthalpy difference of –1.95 kJ·mol^{-1}. Ludjibaite is metastable with respect to its polymorph pseudomalachite. Slavkovite is probably restricted to local acidic environments, rich in Cu and As.

Keywords: thermodynamics, crystal structure, zincolivenite, strashimirite, slavkovite, ludjibaite
Received: 4 April 2022; accepted: 8 December 2022; handling editor: F. Laufek
The online version of this article (doi: 10.3190/jgeosci.367) contains electronic supplementary material.

1. Introduction

Copper oxysalts form an unusually diverse group of minerals, with many different topologies of heteropolyhedral units and Cu^{2+} coordinations (Eby and Hawthorne 1993; Hawthorne and Schindler 2000). Many copper sulfates, phosphates, and arsenates are known and new minerals from this large group are still being described (e.g., Filatov et al. 2020; Rumsey et al. 2021). The occurrence and properties of these phases prompt the evaluation of thermodynamic stability of these minerals. Some of these minerals are common, for example, olivenite (Southwood et al. 2020). Many sites where copper oxysalts occur are well known for their mineral diversity (i.e., the number of mineral species) and complex paragenetic relations (e.g., Weiland 2013). Because of their extensive polymorphism, these minerals can be used to explore the relationship between their energetics and structural complexity (mathematically defined in Krivovichev et al. 2016, 2017). Synthetic analogues of natural copper oxysalts are being intensely investigated as model systems for frustrated magnetic phenomena (Belik et al. 2007; Fennell et al. 2011). From a geochemical perspective, the principal question is whether the abundance or rarity of a certain mineral can be linked to its stability or is it rather dictated by geochemical or geological factors. The latter may include, for example, buffering of pH by the most abundant aqueous species outside of a stability field of a certain mineral, or geochemical decoupling of certain elements.

The only metal that substitutes for Cu^{2+} in natural oxysalts in larger amounts is Zn. This property is prominent in the carbonates of malachite group (Perchiazzi et al.

2017) where the high Zn concentrations lead to splitting of the structural sites to those preferentially occupied by Cu and those occupied by Zn. Among arsenates, the most common example is the adamite–olivenite solid solution with the intermediate phase zincolivenite (Gołębiowska et al. 2006; Chukanov et al. 2007).

Ludjibaite [$Cu_5(PO_4)_2(OH)_4$] is a less common polymorph of pseudomalachite (Piret and Deliens 1988). There are a few sites where it occurs, occasionally together with a third polymorph reichenbachite (Sieber et al. 1987; Hyršl 1991). Krivovichev et al. (2016) analyzed the structures of the three polymorphs and determined that their structural complexity is similar (3.654 and 3.567 bits/atom for ludjibaite and pseudomalachite, respectively). They concluded that structural complexity in this case is not a factor that influences the stability (or metastability) of one polymorph in preference to another. Ludjibaite, pseudomalachite, and reichenbachite are combinatorial polymorphs and the preference for their formation may lie in the structure of prenucleation clusters or chemical admixtures, but not the slight differences in their structural complexity.

Strashimirite [ideally $Cu_8(AsO_4)_4(OH)_4 \cdot 5H_2O$] is a complex copper arsenate (Mincheva-Stefanova 1968). It is generally considered to be rare, but there are more than 80 localities in Europe where the mineral has been found (Mindat 2022), suggesting that it is an inconspicuous, but perhaps a fairly common minor companion of other copper arsenates. It often occurs together with parnauite [$Cu_9(AsO_4)_2(SO_4)(OH)_{10} \cdot 7H_2O$].

Slavkovite [ideally $Cu_{13}(AsO_4)_6(AsO_3OH)_4 \cdot 23H_2O$] was described by Sejkora et al. (2010) from the Geschieber vein in Jáchymov, Czech Republic. It is a weathering product of chalcopyrite and tennantite and occurs together with geminite [$Cu(AsO_3OH) \cdot H_2O$], lindackerite [$CuCu_4(AsO_4)_2(AsO_3OH)_2 \cdot 9H_2O$], ondrušite [$CaCu_4(AsO_4)_2(AsO_3OH)_2 \cdot 10H_2O$] and an unnamed lavendulan-like mineral phase of an idealized composition $Ca_2Cu_5(AsO_4)_4(OH,Cl)_2 \cdot 7H_2O$. Sejkora et al. (2010) mentioned another site for this mineral, in Krásno, near Horní Slavkov (also Czech Republic), where it formed by weathering of tennantite and cuprite. Slavkovite is associated with clay minerals and X-ray amorphous Cu–Fe arsenates. Later, slavkovite was found also at the Krupka ore district (Czech Republic) in paragenetic sequence strashimirite → unnamed lavendulan-like Cu–Ca arsenate → olivenite → slavkovite → Cu arsenate (probably dehydrated slavkovite) (Sejkora et al. 2015).

2. Samples

2.1. Natural samples

Two natural samples of strashimirite were investigated in this work. The first sample NHS-1 originates from the Bartolomej mining field near Novoveská Huta, Slovakia (GPS coordinates: 48.894524° N, 20.500403° E, format WGS84). On this sample, strashimirite is associated with cornwallite and clinoclase. The supergene minerals were formed by weathering of tennantite hosted in Permian sandstones. The second specimen M28/PD15 originates from the Drienok deposit near Poniky, Slovakia (GPS coordinates 48.709822° N, 19.252075° E). Here, strashimirite is associated with olivenite, devilline, brochantite, and minor gypsum. Strashimirite was formed here during the post-mining weathering of fragments of tennantite ore in an abandoned medieval mine.

The samples of slavkovite come from the holotype specimen from Jáchymov used to describe this mineral, deposited in the Mineralogical collection of the National Museum in Prague with the sample label P1N 83.038. They were described by Sejkora et al. (2010) and an overview of that description was provided above.

2.2. Synthetic samples

The synthetic analogues of adamite, zincolivenite, olivenite, and ludjibaite were prepared in the laboratory at the University Jena. A brief description of their syntheses is outlined below. Additional details and description of the syntheses that did not lead to the desired products can be found in Plumhoff (2021) and Tost (2021).

Adamite was synthesized by a modified wet chemical method following Keller (1971). All solutions were pre-

Tab. 1 Unit-cell parameters of olivenite, adamite, zincolivenite, ludjibaite, strashimirite and dehydrated slavkovite

Phase	Space group	Structural model	*a* (Å)[a]	*b* (Å)	*c* (Å)	α (°)	β (°)	γ (°)
olivenite	$P2_1/n$	Burns and Hawthorne (1995)	8.6426(1)	8.2459(1)	5.9422(1)	90.061(3)		
adamite	*Pnnm*	Jinnouchi et al. (2016)	8.3191(4)	8.5334(5)	6.0551(3)			
zincolivenite	*Pnnm*	Chukanov et al. (2007)	8.4018(5)	8.4951(6)	5.9818(3)			
ludjibaite	$P\bar{1}$	Shoemaker et al. (1981)	4.4506(1)	5.8766(1)	8.6684(1)	103.60(1)	90.29(1)	92.96(1)
strashimirite NHS-1	[b]	Mincheva-Stefanova (1968)	9.698(3)	18.902(6)	9.130(2)		97.09(2)	
strashimirite M28/PD15			9.697(5)	18.905(7)	9.132(5)		97.1(2)	
dehydrated slavkovite	$P\bar{1}$	this work	6.4042(11)	13.495(2)	13.574(2)	87.01(2)	85.56(1)	79.68(2)

[a] Unit-cell parameters constrained by symmetry are not listed

[b] The space group for strashimirite is not known

pared with deionized water. The starting solutions of 100 mL of 0.025 M KH_2AsO_4 and 100 mL 0.025 M $ZnSO_4$ were filled into a borosilicate bottle and heated to 80 °C under constant stirring. The pH was adjusted to 8 with 4 wt. % NaOH solution. The bottle was closed and placed into an oven at 80 °C for seven days. The final product was filtered hot, washed several times with deionized water and air-dried at ambient temperature.

Zincolivenite was synthesized using the same procedure as adamite, except the starting solutions were 100 mL 0.025 M KH_2AsO_4, 50 mL 0.0125 M $ZnSO_4$ and 50 mL 0.0125 M $CuSO_4$, and the pH was adjusted to 7. The solution was held at 80 °C for ten days.

Olivenite was synthesized by mixing 50 mL 0.5 M $Cu(NO_3)_2$ solution with 50 mL 0.19 M Na_2HAsO_4. The solids were initially dissolved in separate volumes of deionized water. The arsenical solution was then poured into the cupric solution and the mixture was stirred while being kept at 70 °C and adjusting pH to 3 using $(NH_4)OH$ (28–30 % NH_3). Once pH stabilized, the mixture was transferred into a borosilicate bottle, tightly closed and placed in a constant-temperature water bath at 70 °C. The pH was controlled and raised with $(NH_4)OH$ (28–30 % NH_3) every few hours. After four days, the resulting suspension was filtered hot, washed several times with deionized water and air-dried at ambient temperature.

Ludjibaite was synthesized by hydrothermal treatment of an aqueous solution prepared at room temperature. The following chemicals were added to 30 mL of deionized water: 0.2454 g $Cu(OH)_2$, 0.5453 g $Cu(CH_3COO)_2 \cdot H_2O$, 2.1229 g of $K_3PO_4 \cdot H_2O$ and 0.5 mL of 85 % H_3PO_4. This mixture was loaded into a Teflon-lined reaction container and held there at 180 °C at saturated vapour pressure for 24 hours. The initial pH of 11.7 dropped to 8.0 at the end of the synthesis (measured at ambient temperature). Afterwards, the container was allowed to cool down in air, the product was filtered, rinsed with a small amount of deionized water and dried at room temperature.

3. Methods

The selection of the methods was dictated by the nature of each of the samples. All samples were initially screened by powder X-ray diffraction that confirmed their conclusive match with the corresponding structure model and their purity. Natural samples, because of their chemical variability, were analyzed for their chemical composition, but the synthetic ones were not. Content of H_2O in the slavkovite was not determined directly (e.g., by thermogravimetry) because of the small amount of material available. In that case (and only in that case), single-crystal X-ray diffraction was used. Therefore, the samples underwent tailored characterization for each of them, so the calorimetric results could be referred to as a well-known structure and composition. The sample aliquots used for calorimetry were exactly those characterized by the appropriate methods.

3.1. X-ray diffraction

Powder X-ray diffraction (pXRD) data of all the solid samples were collected with a Bruker D8 ADVANCE with DAVINCI design, and with Cu Kα radiation, Ni filter, and a Lynxeye 1D detector. A step size of 0.02 °2Θ and 0.25 s per step were used. Unit-cell parameters were refined using the JANA2006 program (Petříček et al. 2014).

Single-crystal XRD data were collected for a green, prismatic (117 × 9 × 8 μm) slavkovite crystal removed directly from the aggregate later used for the calorimetric study. The data were acquired with a Rigaku SuperNova single-crystal diffractometer (Institute of Physics of the CAS, Prague, Czech Republic) equipped with Atlas S2 detector using the mirror-monochromatized MoKα radiation (λ = 0.71073 Å) from a micro-focus X-ray tube, providing a high-flux brilliant beam. Corrections for background, Lorentz effect and polarization were applied to the data during the reduction process in the CrysAlis package (Rigaku). The absorption correction was applied via the multi-scan method implemented in the ABSPACK3 algorithm in the CrysAlis. The unit-cell of the studied slavkovite has been found to be considerably smaller than for the sample studied in the original description, V = 1150 Å^3 (currently studied) *vs.* V = 1442 Å^3 (Sejkora et al. 2010). Unit-cell parameters (Tab. 1) were obtained from the least-squares fitting of 1312 reflections. The structure was solved using an intrinsic-phasing algorithm of the program SHELXT (Sheldrick 2015) and subsequently refined by the least-squares refinement in JANA2020 (Petříček et al. 2020). All relevant structure data are given in the **.cif* file (Electronic Supplementary Material, ESM 1). The overview of the data collection conditions, basic crystallographic parameters and refinement details is given in the Tab. 2. A complete bond-valence analysis is given in ESM 2.

3.2. Electron-microprobe analysis

The chemical composition of both strashimirite samples was quantitatively determined using a Cameca SX100 electron microprobe (Laboratory of Electron Microscopy and Microanalysis of Masaryk University and the Czech Geological Survey in Brno, Czech Republic) operating in the wavelength-dispersive (WDS) mode (15 kV, 10 nA and 10 μm wide beam). The following standards and X-ray lines were used to minimize line overlaps: albite (Na K_α), almandine (Fe K_α), Bi (Bi M_β), celestine (S K_α), Co (Co K_α), fluorapatite (Ca K_α, P K_α), gahnite (Zn K_α), lammerite (Cu K_α, As L_α), Mg_2SiO_4 (Mg K_α), Ni_2SiO_4 (Ni

Tab. 2 Data collection and structure refinement details for dehydrated slavkovite

Chemical formula	$Cu_{12}(AsO_4)_4(AsO_3OH)_6 \cdot 14H_2O$
Crystal system	Triclinic
Space group	$P\bar{1}$
Unit-cell parameters: *a*, *b*, *c* [Å]; α, β, γ [°]	6.4042(11), 13.495 (2), 13.574 (2); 87.009(15), 85.564(14), 79.678(15)
Unit-cell volume [Å^3]	1149.8(3)
Z	1
Calculated density [g cm^{-3}]	3.5226 (for the formula from the structure without H atoms)
Crystal size [mm]	0.117 × 0.009 × 0.008
Diffractometer	Rigaku SuperNova with Atlas S2 CCD
Temperature [K]	298
Radiation, wavelength [Å]	MoK_α, 0.71073 (50 kV, 30 mA)
θ range for data collection [°]	3.01−28.70
Limiting Miller indices	h = –8→8, k = –17→17, l = –17 → 17
Axis, frame width (°), time per frame (s)	ω, 1.0, 650
Total reflections collected	14566
Unique reflections	5005
Unique observed reflections, criterion	2285, [$I > 3\sigma(I)$]
Absorption coefficient [mm^{-1}], type	12.72; multi-scan
T_{min}/T_{max}	0.695/1
Data completeness to θ_{max}, R_{int}	0.86, 0.116
Structure refinement	Full-matrix least-squares on F
No. of param., restraints, constraints	248, 0, 0
R, wR (obs)	0.0910, 0.1619
R, wR (all)	0.2026, 0.1950
GOF obs/all	1.95, 1.55
Weighting scheme, weights	σ, $w = 1/(\sigma^2(I)+0.0004I^2)$
Largest diffraction peak and hole (e$^-$ Å^{-3})	5.84, –3.96

K_α), sanidine (Al K_α, K K_α, Si K_α), Sb (Sb L_β), $ScVO_4$ (V K_α), spessartine (Mn K_α), topaz (F K_α) and vanadinite (Cl K_α , Pb M_α). All these elements were sought; those not explicitly included in the tables were below the detection limit (0.03–0.05 wt. %). Peak counting times (CTs) were 20 s for major elements and 60 s for minor elements; the CT for each background was one-half of the peak time. Raw intensities were converted to the concentrations of elements using automatic "PAP" matrix-correction software (Pouchou and Pichoir 1985).

3.3. ICP-OES chemical analysis

The elemental composition of the synthetic samples was analysed with a simultaneous radial inductively coupled optical emission spectrometer (ICP-OES) 725ES (Agilent, Germany) with CCD-detector and an ASX 520 autosampler (Teledyne CETAC, Omaha, USA). Each sample (~10 mg) was dissolved in 15 mL of 0.5 M HCl.

3.4. Calorimetry

Acid-solution calorimetry on the zincolivenite, adamite, olivenite, ludjibaite, strashimirite, and dehydrated slavkovite samples was undertaken using an IMC-4400 instrument (Calorimetry Sciences Corporation) (Majzlan 2017) at the University Jena. A water reservoir was held at a constant temperature of 298.15 K. After stabilization of the calorimeter overnight, the sample pellet with 10 mg weight was dropped into the solvent (25 g 5 N HCl) held in a PEEK (polyetheretherketone) container. The samples were dissolved in the acid solution; the heat flow between the sample and a reference cell, both immersed in the constant-temperature bath, was measured to calculate the heat of dissolution.

The heat capacity (C_p) of ludjibaite was measured by relaxation calorimetry using a commercial Physical Properties Measurement System (PPMS, from Quantum Design, San Diego, California). With due care, the accuracy can be within 1 % from 5 K to 300 K, and 5 % from 0.7 K to 5 K (Kennedy et al. 2007). Powdered samples were wrapped in a thin Al foil and compressed to produce an about 0.5 mm thick pellet which was then placed onto the sample platform of the calorimeter for measurement. The heat capacity was measured in the PPMS in a 2–300 K temperature interval.

4. Results

4.1. Chemical composition and crystal structures

The chemical composition of olivenite, zincolivenite, and adamite was determined by ICP-OES and the results are listed in Tab. 3. The relative proportions of the cations (Cu/Zn) differ little from the initial ratios in the parental solutions. The composition determined for our zincolivenite samples is $Cu_{0.95}Zn_{1.05}(AsO_4)(OH)$. The composition of our adamite sample is $Zn_2(AsO_4)(OH)$. Unit-cell parameters of these phases are listed in Tab. 1 and agree well with those previously reported by Chukanov et al. (2007) for zincolivenite and by Hill (1976), Kato and Miúra (1977), Jinnouchi et al. (2016) for adamite.

The strashimirite and slavkovite phases appeared to be homogeneous in back-scattered electron images. The

strashimirite analyses (Tab. 3) were compromised owing to their porosity and a poor polish. Even though both samples were confirmed by pXRD, by means of correlating to published unit-cell parameters (Tab. 1), the ratios of the main elements, especially Cu/As, were different and neither of them conformed to end-member compositions. The ideal formula of strashimirite is $Cu_8(AsO_4)_4(OH)_4 \cdot 5H_2O$, with Cu/As atomic ratio of 2. The sample from Drienok (M28/PD15), assuming some substitution of Zn for Cu and S for As, has the atomic ratio (Cu+Zn)/(As+S) of 1.96. For the sample from Novoveská Huta (NHS-1), the atomic ratio (Cu+Zn)/(As+Sb+P) is 2.41, much higher than the ideal value of 2. For this reason, thermodynamic data are presented only for the sample from Drienok, and we note that there is a need to further investigate the complexity of the strashimirite structure. The determined formula for the Drienok sample is $(Cu_{7.75}Zn_{0.09})_{7.84}(AsO_4)_{3.89}(SO_4)_{0.11}(OH)_{3.79} \cdot 5H_2O$, with the corresponding molar mass of 1203.86 g·mol^{-1}. Because of the small amount of the sample, H_2O content was not analyzed but assumed to be equal to the nominal value.

Tab. 3 Chemical composition of the synthetic olivenite, adamite, and zincolivenite samples (wt. %)

	olivenite[a]	adamite[a]	zincolivenite[a]	strashimirite M28/PD15 avg(std)[b]	strashimirite NHS–1 avg(std)[b]
FeO	–	–	–	0.18(9)	bdl
CaO	–	–	–	0.21(2)	bdl
CuO	59.94	bdl	28.19	51.84(71)	56.73(78)
ZnO	bdl	59.36	31.06	0.63(3)	0.26(8)
Al_2O_3	–	–	–	0.13(2)	bdl
As_2O_5	39.70	38.39	39.68	37.59(34)	33.31(57)
SO_3	–	–	–	0.75(4)	bdl
P_2O_5	–	–	–	bdl	0.10(7)
SiO_2	–	–	–	bdl	0.15(10)
Sb_2O_5	–	–	–	bdl	0.79(37)
Total	99.63	97.75	98.93	91.33(66)	91.35(87)

[a] The oxide components calculated from ICP-OES results on aqueous solutions produced from the samples. – = not analyzed.

[b] Chemical composition determined by electron microprobe. All other analyzed elements (Na, K, Mg, Pb, Co, Ni, Mn, Bi, V, Cl, F) were always below detection limit (bdl). avg(std) = mean with one standard deviation on the last decimal digit(s) in the parentheses.

The ludjibaite sample was not analyzed chemically. It was assumed that the synthetic product, confirmed by pXRD, corresponds to the nominal composition. Unit-cell parameters for the sample are listed in Tab. 1. Many samples were prepared, with slight variations of the synthesis conditions described above, which produced often pseudomalachite and/or reichenbachite impurities. An impurity-free sample was chosen for the calorimetry.

The sample of slavkovite used in this work originated from the holotype material used in the description of the mineral by Sejkora et al. (2010). These authors concluded that substitutions on the Cu and As sites are negligible, and the chemical formula should be essentially $Cu_{13}(AsO_4)_6(AsO_3OH)_4 \cdot 23H_2O$.

A slight colour change of this material indicated that some chemical changes have occurred meanwhile; the most likely being the change in the number of H_2O molecules per formula unit. Due to the lack of sample, the crystals selected for calorimetry were investigated using single-crystal X-ray diffraction methods to better determine H_2O content, as the thermogravimetric analysis was not possible. The H_2O content was quantified by the refinement of the occupancies of oxygen atoms that belong to OH or H_2O groups in the structure. Single-crystal X-ray diffraction data revealed a significantly smaller unit-cell volume than that reported by Sejkora et al. (2010). Refinement of the data led to an idealized structural formula of $Cu_{12}(AsO_4)_4(AsO_3OH)_6 \cdot 14H_2O$ (molar mass: 2410.008 g·mol^{-1}), confirming the significant loss of H_2O.

Structurally, the dehydration, which has occurred over a period of approximately 10 years at room temperature, has been connected to the collapse of the slavkovite sheet structure into a framework with channels and a reorganization of the bonding (Fig. 1), resulting in a loss of ~8 H_2O. The major structural differences are manifested by the protonation of some of the originally unprotonated AsO_4 groups in slavkovite. The resulting phase will be referred to hereafter as 'dehydrated slavkovite' to differentiate it clearly from the higher hydrate, the actual slavkovite as defined by Sejkora et al. (2010). The 'dehydrated slavkovite' was investigated in the current work; we found that all available specimens of original slavkovite had been similarly affected.

4.2. Calorimetry

4.2.1. Standard enthalpies at 298.15 K

All samples and reference phases dissolved rapidly and reproducibly in the solvent. The dissolution of the samples is described by reactions 1–6 in Tab. 4. The measured enthalpies of dissolution and the formation enthalpies of the reference phases are summarized in Tab. 5.

The enthalpies of formation from elements in their standard state at $T = 298.15$ K and $P = 10^5$ Pa of adamite (ΔH_{23}) and zincolivenite (ΔH_{24}) were calculated from a thermochemical cycle, involving chemical reactions and the reference-phase enthalpies (Tabs 4–5) as

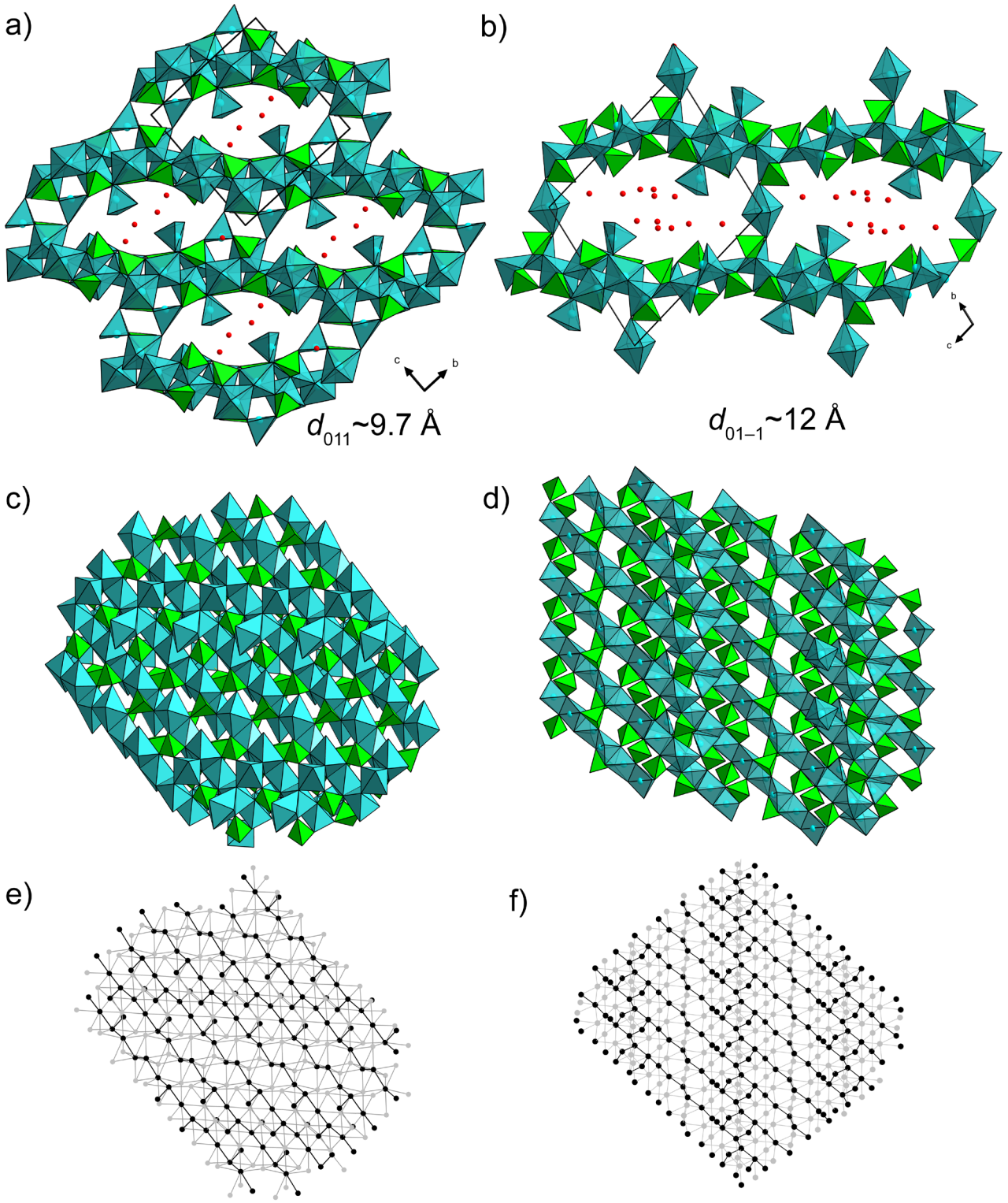

Fig. 1 Crystal structures of **a –** dehydrated slavkovite (current study) and **b –** slavkovite (Sejkora et al. 2010). The corresponding "*interplanar*" distance is shown. The single copper–arsenate layer is shown for dehydrated slavkovite **(c)** and slavkovite **(d),** along with the graph representations of their topologies (e and f, respectively). Colour scheme: As-tetrahedra = green, As atoms = grey, As–Cu bonds = grey, Cu-polyhedra = azure, Cu atoms = black, Cu–Cu bonds = black bold, O atoms of the H_2O groups = red.

$$\Delta_f H^o(\text{adamite}) = 2\Delta H_9 + \Delta H_7 + \Delta H_{11} - \Delta H_2 - \Delta H_{13} - 10.96\Delta H_{12} + 2\Delta H_{17} + \Delta H_{15} + \Delta H_{19} - \Delta H_{21} - 10.96\Delta H_{20} \quad 28$$

$$\Delta_f H^o(\text{zincolivenite}) = 0.95\Delta H_{10} + 1.05\Delta H_9 + \Delta H_7 + \Delta H_{11} - \Delta H_3 - \Delta H_{13} - 10.96\Delta H_{12} + 0.95\Delta H_{18} + 1.05\Delta H_{17} + \Delta H_{15} + \Delta H_{19} - \Delta H_{21} - 10.96\Delta H_{20} \quad 29$$

The calculated $\Delta_f H^o$(adamite) = -1401.7 ± 2.6 kJ·mol^{-1} and $\Delta_f H^o$(zincolivenite) = -1211.6 ± 3.2 kJ·mol^{-1} (Tab. 6).

The enthalpy of zincolivenite relative to a mechanical mixture of olivenite and adamite, i.e., the enthalpy for the reaction 0.475 $Cu_2(AsO_4)(OH)$ + 0.525$Zn_2(AsO_4)(OH)$ → $Cu_{0.95}Zn_{1.05}(AsO_4)(OH)$ can be calculated as:

$$\Delta H_{30} = (0.95/2)\Delta H_1 + (1.05/2)\Delta H_2 - \Delta H_3 \quad 30$$

and amounts to -1.95 ± 0.25 kJ·mol^{-1}.

The dissolution of the ludjibaite, strashimirite, and dehydrated slavkovite samples is described by reactions 4–6 and the corresponding formation reactions 25–27 are listed in Tab. 4. The enthalpies of formation, calculated from the appropriate thermochemical cycles, are summarized in Tab. 6. The corresponding equations for the calculation of the enthalpies of formation are:

$$\Delta H_{25} = \Delta_f H^o(\text{ludjibaite}) = 2\Delta H_8 + 5\Delta H_{10} + 2\Delta H_{11} - \Delta H_4 - 20.92\Delta H_{12} - 2\Delta H_{13} + 2\Delta H_{16} + 5\Delta H_{18} + 2\Delta H_{19} - 2\Delta H_{21} - 20.92\Delta H_{20} \quad 31$$

$$\Delta H_{26} = \Delta_f H^o(\text{strashimirite}) = 0.11\Delta H_{14} + 7.64\Delta H_{10} + 0.09\Delta H_9 + 3.89\Delta H_7 + 3.89\Delta H_{11} - \Delta H_5 - 3.89\Delta H_{13} - 38.2344\Delta H_{12} + 0.11\Delta H_{22} + 7.64\Delta H_{18} + 0.09\Delta H_{17} + 3.89\Delta H_{15} + 3.89\Delta H_{19} - 3.89\Delta H_{21} - 38.2344\Delta H_{20} \quad 32$$

$$\Delta H_{27} = \Delta_f H^o(\text{dehydrated slavkovite}) = 12\Delta H_{10} + 10\Delta H_7 + 10\Delta H_{11} - \Delta H_6 - 10\Delta H_{13} - 97.6\Delta H_{12} + 12\Delta H_{18} + 10\Delta H_{15} + 10\Delta H_{19} - 10\Delta H_{21} - 97.6\Delta H_{20} \quad 33$$

Tab. 4 Dissolution and formation reactions for the studied samples and reference phases

$Cu_2(AsO_4)(OH)$ (cr) + H^+ (aq) → $2Cu^{2+}$ (aq) + AsO_4^{3-} (aq) + H_2O	1
$Zn_2(AsO_4)(OH)$ (cr) + H^+ (aq) → $2Zn^{2+}$ (aq) + AsO_4^{3-} (aq) + H_2O	2
$Cu_{0.95}Zn_{1.05}(AsO_4)(OH)$ (cr) + H^+ (aq) → $0.95Cu^{2+}$ (aq) + $1.05Zn^{2+}$ (aq) + AsO_4^{3-} (aq) + H_2O	3
$Cu_5(PO_4)_2(OH)_4$ (cr) + $4H^+$ (aq) → $5Cu^{2+}$ (aq) + $2PO_4^{3-}$ (aq) + $4H_2O$ (aq)	4
$(Cu_{7.75}Zn_{0.09})(AsO_4)_{3.89}(SO_4)_{0.11}(OH)_{3.79}\cdot 5H_2O$ (cr) + $3.79H^+$ (aq) → $7.75Cu^{2+}$ (aq) + $0.09Zn^{2+}$ (aq) + $3.89AsO_4^{3-}$ (aq) + $0.11SO_4^{2-}$ (aq) + $8.79H_2O$	5
$Cu_{12}(AsO_4)_4(AsO_3OH)_6\cdot 14H_2O$ (cr) → $12Cu^{2+}$ + $10AsO_4^{3-}$ + $6H^+$ + $14H_2O$	6
KH_2AsO_4 (cr) → K^+ (aq) + $2H^+$ (aq) + AsO_4^{3-} (aq)	7
KH_2PO_4 (cr) → K^+ (aq) + $2H^+$ (aq) + PO_4^{3-} (aq)	8
ZnO (cr) + $2H^+$ (aq) → Zn^{2+} (aq) + H_2O (aq)	9
CuO (cr) + $2H^+$ (aq) → Cu^{2+} (aq) + H_2O (aq)	10
$HCl\cdot 9.96H_2O$ (l) → H^+ (aq) + Cl^- (aq) + $9.96H_2O$ (aq)	11
H_2O (l) → H_2O (aq)	12
KCl (cr) → K^+ (aq) + Cl^- (aq)	13
$CuSO_4\cdot 5H_2O$ (cr) → Cu^{2+} (aq) + SO_4^{2-} (aq) + $5H_2O$ (aq)	14
K (cr) + As (cr) + H_2 (g) + $2O_2$ (g) → KH_2AsO_4 (cr)	15
K (cr) + P (cr) + H_2 (g) + $2O_2$ (g) → KH_2PO_4 (cr)	16
Zn (cr) + $0.5O_2$ (g) → ZnO (cr)	17
Cu (cr) + $0.5O_2$ (g) → CuO (cr)	18
$10.46H_2$ (g) + $4.98O_2$ (g) + $0.5Cl_2$ (g) → $HCl\cdot 9.96H_2O$ (l)	19
H_2 (g) + $0.5O_2$ (g) → H_2O (l)	20
K (cr) + $0.5Cl_2$ (g) → KCl (cr)	21
Cu (cr) + S (cr) + $4.5O_2$ (g) + $5H_2$ (g) → $CuSO_4\cdot 5H_2O$ (cr)	22
2Zn (cr) + As (cr) + $0.5H_2$ (g) + $2.5O_2$ (g) → $Zn_2(AsO_4)(OH)$ (cr)	23
0.95Cu (cr) + 1.05Zn (cr) + As (cr) + $0.5H_2$ (g) + $2.5O_2$ (g) → $Cu_{0.95}Zn_{1.05}(AsO_4)(OH)$ (cr)	24
5Cu + 2P + $6O_2$ + $2H_2$ → $Cu_5(PO_4)_2(OH)_4$ (cr)	25
$7.75Cu + 0.09Zn + 3.89As + 0.11S + 12.395O_2 + 6.895H_2$ → $(Cu_{7.75}Zn_{0.09})(AsO_4)_{3.89}(SO_4)_{0.11}(OH)_{3.79}\cdot 5H_2O$	26
$12Cu + 10As + 27O_2 + 17H_2$ → $Cu_{12}(AsO_4)_4(AsO_3OH)_6\cdot 14H_2O$	27

4.2.2. Heat capacities and entropies

The heat capacity data for ludjibaite are presented in Fig. 2, together with the C_p data for its polymorph pseudomalachite. As expected, the two C_p sets are numerically close to each other, resulting also in similar entropies. The calculated S^o(ludjibaite) at T = 298.15 K is 389.0 ± 2.7 J·mol^{-1}·K^{-1}. Both phases show broad low-temperature anomalies resulting from the magnetic ordering of Cu^{2+} ions. For ludjibaite, the anomaly is centred

Tab. 5 Dissolution enthalpies of all measured samples and reference phases and formation enthalpies of the reference phases (kJ mol^{-1})

Phase	Dissolution enthalpies	Formation enthalpies
olivenite	$\Delta H_1 = -25.20 \pm 0.31$	
adamite	$\Delta H_2 = -47.05 \pm 0.14$	
zincolivenite	$\Delta H_3 = -34.72 \pm 0.19$	
ludjibaite	$\Delta H_4 = -108.81 \pm 1.06$	
strashimirite	$\Delta H_5 = -116.66 \pm 1.01$	
deh. slavkovite	$\Delta H_6 = 3.82 \pm 0.27$	
KH_2AsO_4 (cr)	$\Delta H_7 = 24.75 \pm 0.18$	$\Delta H_{15} = -1181.2 \pm 2.0$[b]
KH_2PO_4 (cr)	$\Delta H_8 = 25.11 \pm 0.33$	$\Delta H_{16} = -1573.6 \pm 1.0$[b]
ZnO (cr)	$\Delta H_9 = -70.24 \pm 0.11$	$\Delta H_{17} = -350.5 \pm 0.3$[c]
CuO (cr)	$\Delta H_{10} = -51.53 \pm 0.16$	$\Delta H_{18} = -156.1 \pm 2.0$[c]
$HCl\cdot 9.96H_2O$ (l)	$\Delta H_{11} = 0$	$\Delta H_{19} = -3007.9 \pm 1.0$[b]
H_2O (l)	$\Delta H_{12} = -0.54$[a]	$\Delta H_{20} = -285.8 \pm 0.1$[c]
KCl (cr)	$\Delta H_{13} = 17.69 \pm 0.06$	$\Delta H_{21} = -436.5 \pm 0.2$[c]
$CuSO_4\cdot 5H_2O$ (cr)	$\Delta H_{14} = 49.71 \pm 0.19$	$\Delta H_{22} = -2279.5 \pm 3.4$[d]

[a] calculated from Parker (1965)
[b] see Majzlan (2017)
[c] Robie and Hemingway (1995)
[d] Grevel and Majzlan (2011)

Tab. 6 Thermodynamic properties determined in this work for Cu–Zn secondary minerals

	$\Delta_f H^o$ [a]	S^o [b]	$\Delta_f S^o$ [c]	$\Delta_f G^o$ [a]	log K_{sp} [d]
adamite	–1401.7 ± 2.6				
zincolivenite	–1211.6 ± 3.2				
ludjibaite	–3214.3 ± 10.7	389.0 ± 2.7	–1351.1 ± 2.8	–2811.4 ± 10.7	–24.1
strashimirite	–5374.9 ± 18.1	(835.3)	–3011.5	–4477.0 ± 18.3	–4.5
deh. slavkovite	–12004 ± 34	(1751)	–6764	–9987 ± 35	–54.5

All enthalpy and Gibbs free energy values are in kJ·mol^{-1}, all entropy values are in J·mol^{-1}·K^{-1}.

[a] The formation reactions of the Cu–Zn arsenates and phosphates are defined by reactions 23–27 in Tab. 4.

[b] Estimated values are in parentheses.

[c] Entropies of formation calculated from the listed entropy values and the entropies of elements in their standard state are from Robie and Hemingway (1995).

[d] Solubility products were calculated with these auxiliary data (all in kJ·mol^{-1}): $\Delta_f G^o(Cu^{2+}, aq)$ = +65.1 ± 0.1, $\Delta_f G^o(Zn^{2+}, aq)$ = –147.3 ± 0.2 (Robie and Hemingway 1995), $\Delta_f G^o(HAsO_4^{2-}, aq)$ = –713.73 ± 0.35 (Nordstrom et al. 2014), $\Delta_f G^o(SO_4^{2-}, aq)$ = –744.0 ± 0.4 (Nordstrom and Munoz 1994), $\Delta_f G^o(PO_4^{3-}, aq)$ = –1025.5 ± 1.6 (Grenthe et al. 1992), $\Delta_f G^o(H_2O,l)$ = –237.14 ± 0.04 (Robie and Hemingway 1995).

These equilibrium constants refer to the reactions:

$Cu_3(PO_4)_2(OH)_4 + 4H^+ \rightarrow 5Cu^{2+} + 2PO_4^{3-} + 4H_2O$

$(Cu_{7.75}Zn_{0.09})(AsO_4)_{3.89}(SO_4)_{0.11}(OH)_{3.79}\cdot 5H_2O + 7.68H^+ \rightarrow 7.75Cu^{2+} + 0.09Zn^{2+} + 3.89HAsO_4^{2-} + 0.11SO_4^{2-} + 8.79H_2O$

$Cu_{12}(AsO_4)_4(AsO_3OH)_6\cdot 14H_2O + 4H^+ \rightarrow 12Cu^{2+} + 10HAsO_4^{2-} + 14H_2O$

at ~25 K, and that of pseudomalachite at 5.8 K (Fig. 2b; Majzlan et al. 2015).

Entropy estimates for strashimirite and dehydrated slavkovite were calculated from hypothetical reactions that involve solid phases only. It was assumed that the overall entropy change of that reaction was zero. This is the Kopp–Neumann rule, implying that the entropy of a complex solid equals the sum of entropies of its oxide components, either real or hypothetical. Standard entropies of CuO, ZnO, and As_2O_5 were taken from Robie and Hemingway (1995). The entropy for H_2O(cr) at T = 298.15 K was determined by a sum of Debye and Einstein functions (Majzlan et al. 2003) as 41.94 J mol^{-1} K^{-1}. The entropy of SO_3(cr) was estimated by applying the Kopp–Neumann rule to the pairs of solids MgO–$MgSO_4$, CaO–$CaSO_4$, SrO–$SrSO_4$, and BaO–$BaSO_4$, taking all data from Robie and Hemingway (1995). The resulting value of $S^o(SO_3,cr)$ is 63.9 ± 4.1 J mol^{-1} K^{-1}.

The accuracy of such estimates can be judged from the comparison with experimentally measured entropies. For pseudomalachite or ludjibaite, the deviation is relatively large, ~18 J mol^{-1} K^{-1}, equal to a difference of 5.5 kJ mol^{-1} in $\Delta_f G^o$ at room temperature. For the chemically similar libethenite, however, the difference is only 1.1 J mol^{-1} K^{-1}, equal only to 0.3 kJ mol^{-1} in $\Delta_f G^o$ at room temperature. The magnitude of these deviations can be potentially large enough to alter details in the stability among of the phases studied here. This limitation must be born in mind when considering our results or using the data presented here for geochemical modeling.

The entropy of strashimirite (with the composition of the sample used for calorimetry) was calculated from the reaction:

$$(Cu_{7.75}Zn_{0.09})(AsO_4)_{3.89}(SO_4)_{0.11}(OH)_{3.79}\cdot 5H_2O \rightarrow 7.75CuO + 0.09ZnO + 0.11SO_3 + 1.945As_2O_5 + 6.895H_2O \quad (34)$$

leading to S^o(strashimirite) = 835.3 J mol^{-1} K^{-1}. The entropy of dehydrated slavkovite was calculated from the reaction:

$$Cu_{12}(AsO_4)_4(AsO_3OH)_6\cdot 14H_2O \rightarrow 12CuO + 5As_2O_5 + 17H_2O \quad (35)$$

leading to S^o(dehydrated slavkovite) = 1751.4 J mol^{-1} K^{-1}.

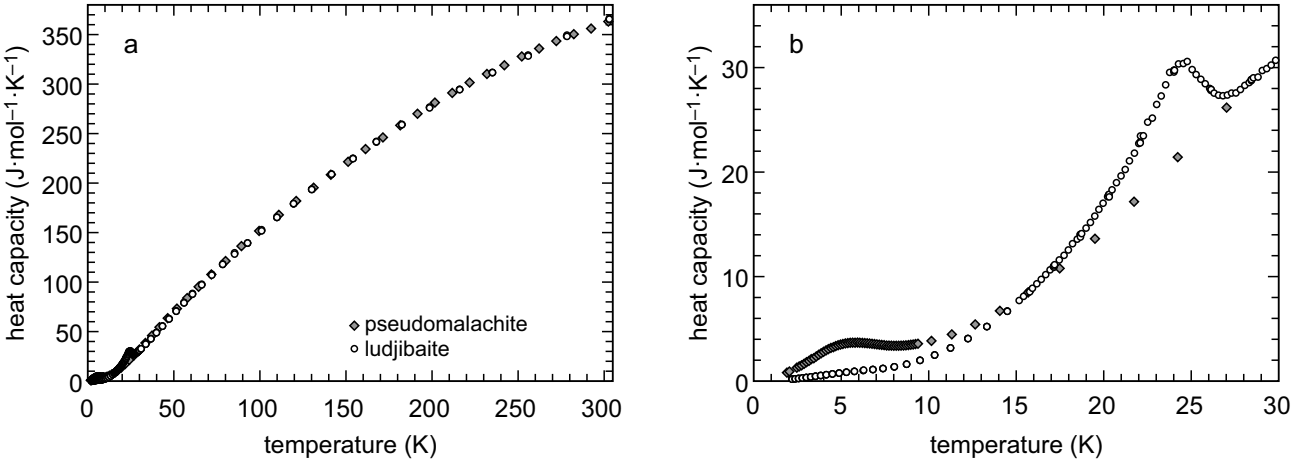

Fig. 2 Comparison of heat capacity of the polymorphs pseudomalachite and ludjibaite. Data for pseudomalachite from Majzlan et al. (2015). **a** – the entire measurement range 2–300 K; **b –** low-temperature data 2–30 K.

5. Discussion

5.1. Ordering in and stability of zincolivenite

Zincolivenite was defined as an ordered Cu–Zn derivative of the olivenite structure (Chukanov et al. 2007). These authors defined the compositional range for zincolivenite from $Cu_{0.5}Zn_{1.5}(AsO_4)(OH)$ to $Cu_{1.5}Zn_{0.5}(AsO_4)(OH)$ and recognized the phase as a new mineral because of Cu/Zn ordering. The actual state of ordering is difficult to quantify because of the similar scattering power of Cu and Zn. Chukanov et al. (2007) assumed ordering based only on missing features in infrared spectra. Their structural model did not prove the presence of ordering. It merely assigned Cu and Zn to two different sites, even though Cu and Zn cannot be distinguished from the conventional XRD data.

We did not conduct experiments that could confirm or refute the ordering in our work. However, the small negative enthalpy relative to adamite and olivenite we calculated, $\Delta H_{30} = -1.95$ kJ mol^{-1}, could be an indicator of structural relief caused by ordering of the Cu/Zn cations on the available octahedral sites. Further work, utilizing anomalous X-ray diffraction (AXRD) would be needed to prove cation ordering in zincolivenite.

5.2. Stability of ludjibaite versus pseudomalachite

Ludjibaite is markedly less common in nature than its polymorph pseudomalachite. The data from this work and those in Majzlan et al. (2015) define the properties of the reaction:

$$\underset{\text{ludjibaite}}{Cu_5(PO_4)_2(OH)_4} \rightarrow \underset{\text{pseudomalachite}}{Cu_5(PO_4)_2(OH)_4} \quad 36$$

with $\Delta_r G^\circ_{36} = -26.5 \pm 15.2$ kJ·mol^{-1}. The enthalpy of transformation, calculated directly from the calorimetric data, is $\Delta_r H^\circ_{36} = -25.4 \pm 1.2$ kJ·mol^{-1}. When energies are normalized to a formula with 1 metal (Cu) atom, i.e., $Cu(PO_4)_{0.4}(OH)_{0.8}$), they both amount to ~ –5 kJ·mol^{-1}. Such energy differences are typical for polymorphs that form and persist over pedogenic or geological time scales (e.g., Navrotsky et al. 2008). Hence, pseudomalachite is the stable polymorph, as expected. Our syntheses yielded consistently pseudomalachite, with larger or smaller amounts of ludjibaite, and only traces of reichenbachite. It could be therefore assumed that reichenbachite is metastable with respect to ludjibaite, although quantification is not possible at the moment.

The entropies of polymorphs are usually similar to each other. In this case, the measured entropy of ludjibaite is 389.0 ± 2.7 J·mol^{-1}·K^{-1} resembles that of pseudomalachite 392.7 ± 4.5 J·mol^{-1}·K^{-1} (Majzlan et al. 2015). The two values overlap within their experimental errors. Pseudomalachite is stabilized with respect to ludjibaite by a significant enthalpy difference (see reaction 36 and its enthalpy above).

5.3. Stability of strashimirite

Strashimirite is closely related in its chemical composition to olivenite and euchroite. Rewriting the nominal formula $Cu_8(AsO_4)_4(OH)_4 \cdot 5H_2O$ as $Cu_2(AsO_4)(OH) \cdot 1.25H_2O$ shows that it is an intermediate hydrate of $Cu_2(AsO_4)(OH)$, between olivenite and euchroite. To these two minerals, strashimirite is related by simple reactions

$$Cu_8(AsO_4)_4(OH)_4 \cdot 5H_2O \text{ (strashimirite)} + 7H_2O \text{ (liquid)} \rightarrow 4Cu_2(AsO_4)(OH) \cdot 3H_2O \text{ (euchroite)} \quad 37$$

$$Cu_8(AsO_4)_4(OH)_4 \cdot 5H_2O \text{ (strashimirite)} \rightarrow 4Cu_2(AsO_4)(OH) \text{ (olivenite)} + 5H_2O \text{ (liquid)} \quad 38$$

The data of Magalhães et al. (1988) and Majzlan et al. (2017) showed that euchroite is metastable with respect to olivenite, for the reaction

$$Cu_2(AsO_4)(OH) \text{ (olivenite)} + 3H_2O \text{ (liquid)} \rightarrow Cu_2(AsO_4)(OH) \cdot 3H_2O \text{ (euchroite)} \quad 39$$

with $\Delta_r G^\circ_{39} = +12.2$ kJ·mol^{-1}. A direct comparison with strashimirite is difficult because the natural sample used in the current work does not perfectly correspond to the nominal composition. A reaction with aqueous ions can be considered, such as

$$(Cu_{7.75}Zn_{0.09})(AsO_4)_{3.89}(SO_4)_{0.11}(OH)_{3.79} \cdot 5H_2O + 0.03Cu^{2+} \rightarrow 3.89Cu_2(AsO_4)(OH) + 0.09Zn^{2+} + 0.11SO_4^{2-} + 0.1H^+ + 5H_2O \quad 40$$

The actual Gibbs free energy difference of reaction 40 also depends on pH and activities of aqueous ions, which makes the discussion of equilibrium difficult. Figure 3 illustrates a set of pH–pε diagrams calculated for specific aqueous ion activities. In this figure, the most stable phase was successively removed (suppressed) from the calculations in order to visualize the stability field of the next metastable phase. The stable copper arsenate is olivenite, followed by cornubite and clinoclase. As expected, with decreasing stability of a copper arsenate, its stability field shrinks at the expense of the flanking stability fields of Cu^{2+}(aq) and tenorite. Under such a condition, strashimirite is metastable with respect to almost all copper arsenates. As such, it is informative to review different natural occurrences of the mineral.

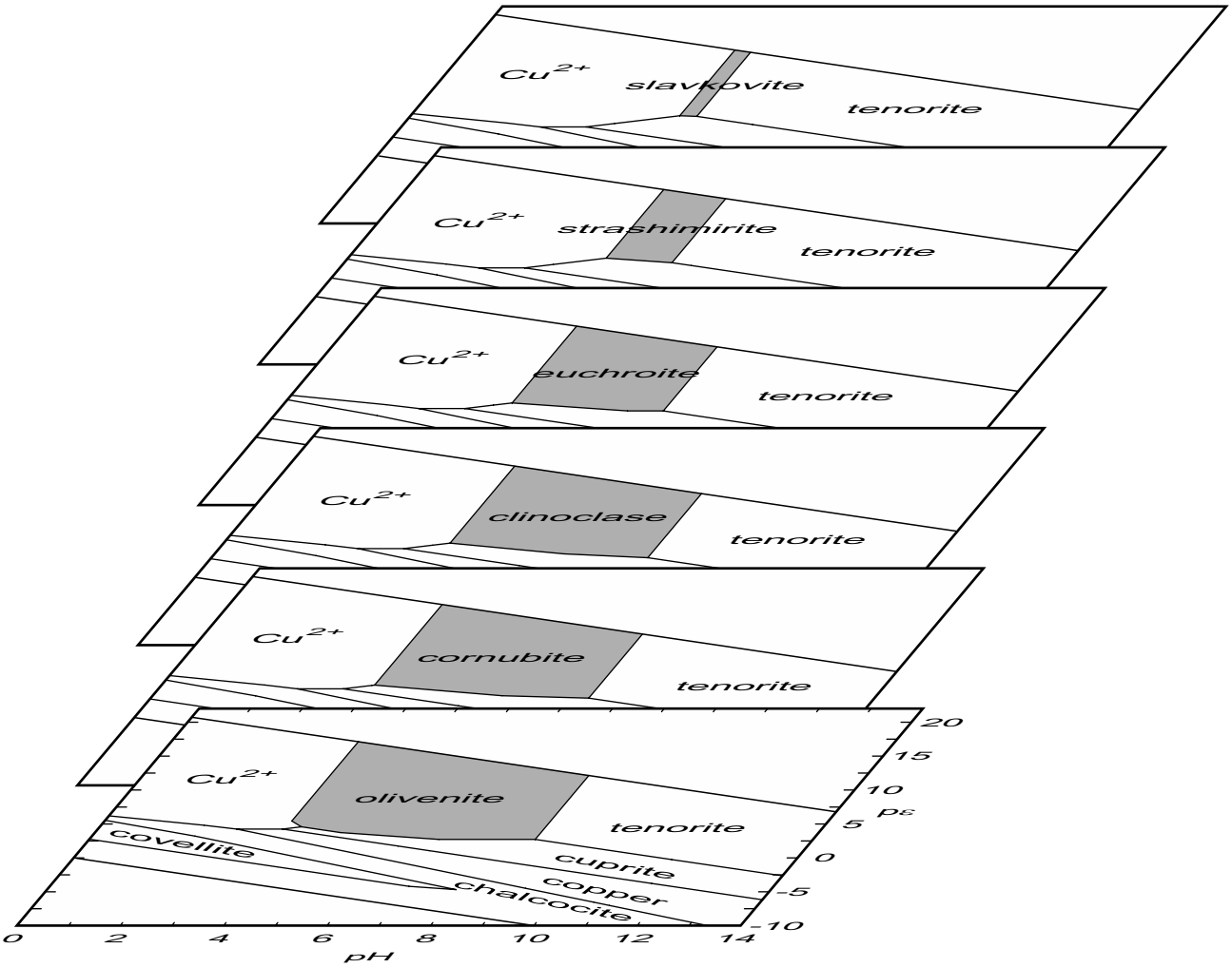

Fig. 3 Stacked pH–pε diagrams for the system Cu–As–O–H, with log *a*(Cu) = –3, log *a*(As) = –3, log *a*(S) = –4, log *a*(Zn) = –5 at *T* = 298.15 K (calculated with Geochemist's Workbench, see Bethke 2022 for the details). The aqueous species of Cu, As, S, and Zn were allowed to speciate according to the pH and pε conditions. Sulfur and Zn were only included in order to plot the field of strashimirite in these diagrams. Lammerite and the Cu sulfates posnjakite, antlerite, brochantite, langite, chalcanthite were suppressed from all calculations. The most stable Cu arsenate is olivenite. In every successive step, the Cu arsenate with a stability field was suppressed from the calculations in order to reveal the field of the next metastable phase.

The most common supergene minerals directly associated with strashimirite are other copper arsenates such as olivenite, cornubite/cornwallite, or clinoclase. At the Svätodušná and Farbište deposits in Slovakia (Fig. 4), strashimirite is always older than the associated olivenite and euchroite (Fig. 4a–b) or clinoclase (e.g., as observed in our samples from Farbište, Driekyňa and Novoveská Huta – Slovakia; Majuba Hill – USA). The oxidation zones at Svätodušná, Farbište, and Driekyňa are localized in schists and acidic–intermediate volcanic rocks (Koděra et al. 1990), that is, rocks with little or no buffering capacity. The main primary ore mineral was tennantite.

We assume that strashimirite crystallizes early during unbuffered oxidative decomposition of tennantite, when the Cu and As concentrations in the descending water build up and reach the highest values. As the weathering proceeds, a steady state is established between decomposition/dissolution and precipitation rates, and the Cu/As concentrations in the fluid are sufficient only for more stable phases.

At Novoveská Huta, pseudomorphs or partial replacements of tangdanite/tyrolite by younger strashimirite (later overgrown by cornwallite and clinoclase) have been observed (Fig. 4c). This deposit is hosted by Permian sedimentary rocks, including sandstones locally impregnated with Cu–U ores and evaporitic rocks with gypsum (Koděra et al. 1990). The main primary ore mineral was tennantite. Such primary mineralogy influenced the early weathering stages and produced Ca-rich (tangdanite and tyrolite), sulfate-rich (chalcophyllite), and U-rich (zeunerite) minerals before the bulk of the copper arsenates precipitated. Here, strashimirite could be a product of the

local re-dissolution of earlier tangdanite/tyrolite and the local increase of Cu/As concentrations in the fluid phase.

There are several examples of post-mining formation of strashimirite in abandoned mines (e.g. Drienok, Slovakia; Jáchymov and Krupka, Czech Republic) or dumps (Schwartzleo, Austria). At the Drienok deposit, strashimirite was formed by weathering of ore fragments (tennantite) in the backfill of a medieval mining tunnel with no flowing water, only under high air humidity. Directly associated minerals are olivenite, rare köttigite–erythrite, as well as common crystalline crusts of brochantite, devilline and minor gypsum (Fig. 4d). Olivenite is always younger here and is growing on aggregates of strashimirite. The assemblages with brochantite, gypsum, and erythrite suggest crystallization from neutral or mildly acidic solutions. Such conditions are not surprising at Drienok because the mineralization is hosted by Middle Triassic dolomites and the host carbonates do not allow the formation of acid mine drainage.

At the Jáchymov deposit, strashimirite is associated with lavendulan, lindackerite, ondrušite, or slavkovite (e.g., Ondruš et al. 1997; Sejkora et al. 2011; Sejkora and Bureš 2020). These minerals precipitate here from acidic solutions where the gangue contains no primary carbonates. The occurrences of these minerals in Jáchymov are relatively scarce. If strashimirite appears, however, it represents the most voluminous phase dominating over the other secondary minerals. Typically, strashimirite occurs in quartz gangue (devoid of carbonates) with disseminated to massive, decomposing tennantite and chalcopyrite. Spatial relationship to other secondary minerals suggests that strashimirite is the oldest phase in the secondary assemblage.

5.4. Stability and formation of dehydrated slavkovite and slavkovite

Slavkovite and dehydrated slavkovite are chemically similar hydrated copper arsenates with different hydration states. The addition of H_2O molecules into a solid state may be approximated by adding the Gibbs free energy of H_2O molecules in liquid water to a less hydrated form (e.g., Hemingway et al. 2002). However, the assumption of constant energy change during successive hydration steps is usually applied to enthalpy rather than Gibbs free energy. Consequently, the entropy during hydration decreases, thus imposing a cooperating or countering factor for enthalpy, leaving Gibbs free energy potentially positive or negative. For this reason, we will not attempt to estimate the thermodynamic properties of slavkovite quantitatively. We will, though, consider the dehydrated slavkovite as a good proxy for the stability of slavkovite.

Under the conditions selected for the construction of Fig. 3, dehydrated slavkovite is the least stable phase, metastable even with respect to strashimirite. The concentrations of the aqueous ions in this figure were selected so that slavkovite appears in one of the diagrams. If the aqueous activities of Cu or As are lowered, slavkovite will have no stability field at all. Under such conditions, there are many competing phases and slavkovite or dehydrated slavkovite could form only at high aqueous Cu and As(V) activities, given that the precipitation of all other minerals is hindered. Such a scenario is unlikely.

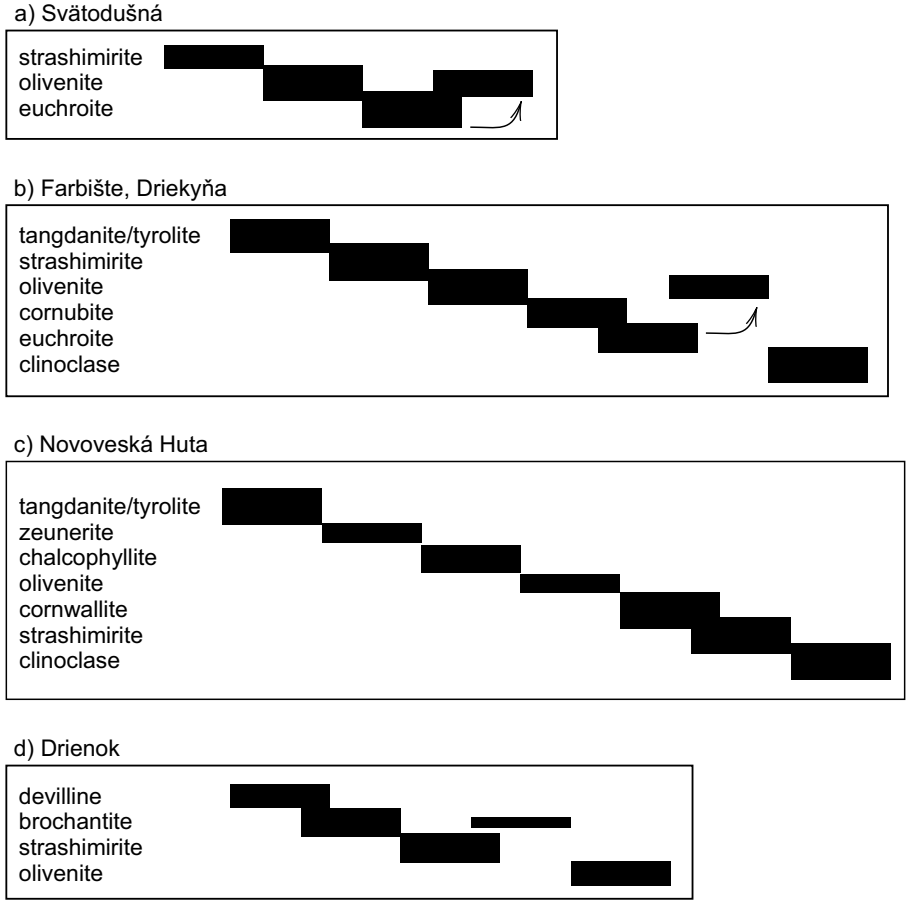

Fig. 4 Precipitation sequence of secondary minerals at several deposits in Slovakia (Svätodušná, Farbište, Driekyňa, , Novoveská Huta and Drienok). The thickness of the bars represents approximately the abundance of the minerals. The arrows show products of solid-state transformation.

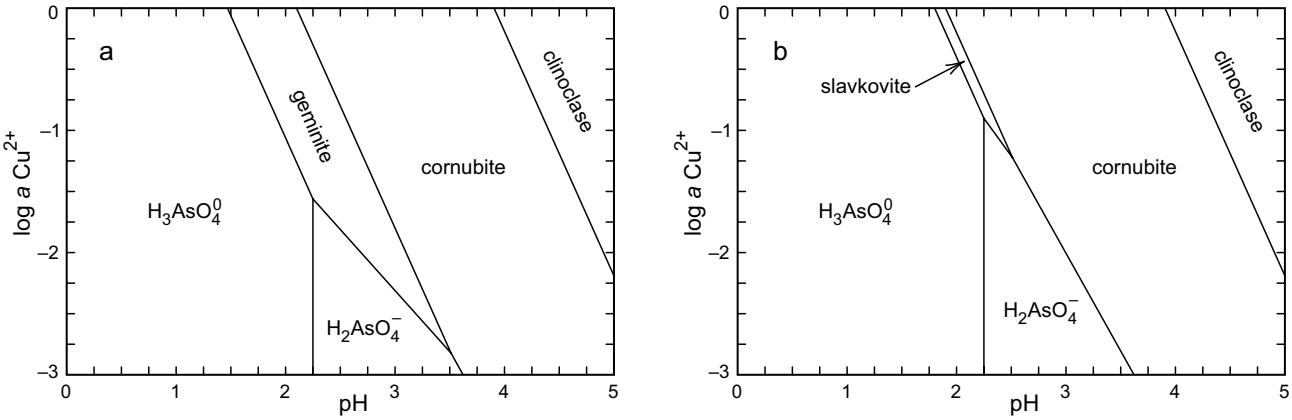

Fig. 5 Activity–activity phase diagrams for the acidic, As- and Cu-rich portion of the system Cu–As–O–H, with log a(As) = –1 at T = 298.15 K (calculated with Geochemist's Workbench, see Bethke 2022 for the details). The aqueous species of As were allowed to speciate according to the pH and pε conditions. **a** – olivenite was suppressed from the calculations; **b** – both olivenite and geminite were suppressed.

There are conditions, however, under which the number of competing phases is small (Fig. 5). Under the acidic conditions, the aqueous activities needed to precipitate solids must be higher, just as those used for the construction of Fig. 5. There, once olivenite is suppressed, the stability field of geminite appears under low pH and high *a*(Cu). Suppression of geminite reveals a small stability field of slavkovite (or dehydrated slavkovite) under similar conditions. Under these conditions, only olivenite and geminite will compete with the formation of slavkovite.

Our data show that dehydrated slavkovite (and likely also slavkovite) is stabilized under acidic conditions and high activities of Cu(II) and As(V) in solution. These conclusions agree well with the field observations and the association of slavkovite with other arsenates with the acidic $AsO_3(OH)$ group in their structure. At the type locality in Jáchymov, such arsenates include geminite, lindackerite, and ondrušite (see above). At the Krupka ore district, slavkovite was formed by recent weathering of tennantite disseminated in greisenized granite in the ceiling of an abandoned mine adit without any water, under high air humidity only (Sejkora et al. 2015). There, slavkovite is distinctly younger than associated strashimirite and olivenite. This situation suggests more acidic conditions and higher activities of Cu and As(V) during slavkovite formation.

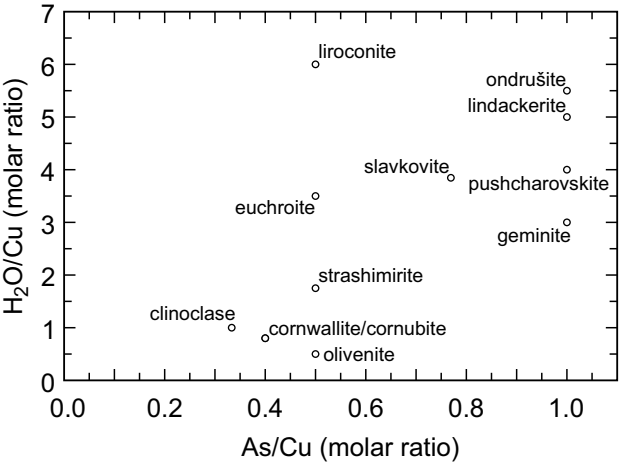

Fig. 6 Molar ratios As/Cu and H_2O/Cu for Cu arsenate minerals.

The As/Cu atomic ratio for slavkovite, geminite, lindackerite and ondrušite also distinguishes them from the olivenite, clinoclase cornwallite/cornubite assemblages (Fig. 6). The atomic As/Cu ratio of the former is substantially greater than 0.5, so it could be assumed that these minerals will be favoured in aqueous solutions with high As/Cu ratios. Under acidic conditions, however, the predominant As(V) species is $H_3AsO_4^0$, meaning that arsenate contributes little to the acidity. Therefore, the environments that precipitate these minerals must be arsenic-rich and develop acidity by oxidation of sulfides to sulfates, as commonly seen in acid-mine drainage. The formation of other minerals, especially olivenite, must be kinetically hindered, and the aqueous Cu and As concentrations must be high enough to form the metastable Cu arsenates. The combination of such multiple prerequisites leads to the rarity of these minerals in nature. It restricts their occurrence to slowly weathering ore veins or ore specimens in mining waste (dumps) without any significant water flow.

6. Conclusions

In this work, we have determined the thermodynamic functions for a suite of Cu–Zn arsenates and phosphates. These data can be used for the purposes of thermodynamic modelling. This work showed that the stable copper arsenate under most conditions is olivenite; less common phases, such as euchroite, strashimirite, or slavkovite are metastable. The degree of metastability can be qualitatively linked to the abundance of these miner-

als in nature. It seems that they form as early, metastable precipitates from highly concentrated aqueous solutions in small microenvironments in mines and mining waste. Owing to their high solubility and transient nature, they are unlikely to limit the solubility of metals and metalloids in mining waste (e.g., tailings) except in the earliest stages of its existence, i.e., shortly after deposition. For long-term modelling, they need not be considered.

Acknowledgments. We thank Mike Rumsey and an anonymous reviewer for their critical comments that significantly improved the manuscript. We are thankful to František Laufek for editorial handling of the manuscript, Alexandra Plumhoff, Felix Tost, Stefanie Notz and Franziska Meißner for the assistance with some of the syntheses and data processing. The work presented here was financially supported by a grant of the *Deutsche Forschungsgemeinschaft* MA 3927/26-1. We acknowledge CzechNanoLab Research Infrastructure supported by MEYS CR (LM2018110) for financial support for the collection of diffraction data.

Electronic supplementary material. The crystallographic information file (CIF) for dehydrated slavkovite and bond-valence analysis of its structure are both available online at the Journal website (*http://dx.doi.org/10.3190/jgeosci.367*).

References

Belik AA, Koo H-J, Whangbo M-W, Tsujii N, Naumov P, Takayama-Muromachi E (2007) Magnetic properties of synthetic libethenite Cu_2PO_4OH: a new spin-gap system. Inorg Chem 46: 8684–8689

Bethke CM (2022) Geochemical and Biogeochemical Modeling, 3rd edition. Cambridge University Press, pp 1–564

Burns PC, Hawthorne FC (1995) Rietveld refinement of the crystal structure of olivenite: a twinned monoclinic structure. Canad Mineral 33: 885–888

Chukanov NV, Pushcharovsky DYu, Zubkova NV, Pekov IV, Pasero M, Merlino S, Möckel S, Rabadanov MKh, Belakovskiy DI (2007) Zincolivenite $CuZn(AsO_4)(OH)$: a new adamite-group mineral with ordered distribution of Cu and Zn. Dokl Russ Acad Sci 415A: 841–845

Eby RK, Hawthorne FC (1993) Structural relations in copper oxysalt minerals. I. Structural hierarchy. Acta Crystall B 49: 28–56

Fennell T, Piatek JO, Stephenson RA, Nilsen GJ, Rønnow HM (2011) Spangolite: an $s = 1/2$ maple leaf lattice antiferromagnet? J Phys Cond Matter 23: 164201

Filatov SK, Shablinskii AP, Krivovichev SV, Vergasova LP, Moskaleva SV (2020) Petrovite, $Na_{10}CaCu_2(SO_4)_8$, a new fumarolic sulfate from the Great Tolbachik fissure eruption, Kamchatka Peninsula, Russia. Mineral Mag 84: 691–698

Gołębiowska B, Pieczka A, Franus W (2006) Olivenite–adamite solid solution from oxidation zone in Rędziny (West Sudetes, Poland). Mineral Pol 37: 101–110

Grenthe I, Fuger J, Konings RJM, Lemire RJ, Muller AB, Nguyen-Trung C, Wanner H (1992) Chemical Thermodynamics of Uranium, volume 1. Nuclear Energy Agency, OECD, pp 1–734

Grevel K–D, Majzlan J (2011) Thermodynamics of divalent metal sulfates. Chem Geol 286: 301–306

Hawthorne FC, Schindler M (2000) Topological enumeration of decorated $[Cu^{2+}\varphi_2]N$ sheets in hydroxy-hydrated copper–oxysalt minerals. Canad Mineral 38: 751–761

Hemingway BS, Seal RR II, Chou I-M (2002) Thermodynamic data for modeling acid mine drainage problems: compilation and estimation of data for selected soluble iron-sulfate minerals. US Geol Surv Open-File Rep 02–161, pp 1–13

Hill RJ (1976) The crystal structure and infrared properties of adamite. Amer Miner 61: 979–986

Hyršl J (1991) Three polymorphs of $Cu_5(PO_4)_2(OH)_4$ from Ľubietová, Czechoslovakia. Neu Jb Mineral, Mh 1991: 281–287

Jinnouchi S, Yoshiasa A, Sugiyama K, Shimura R, Arima H, Momma H, Miyawaki R (2016) Crystal structure refinements of legrandite, adamite, and paradamite: the complex structure and characteristic hydrogen bonding network of legrandite. J Mineral Petrol Sci 111: 35–43

Kato T, Miúra Y (1977) The crystal structures of adamite and paradamite. Mineral J 6: 320–328

Keller P (1971) Darstellung und Eigenschaften von $Co_2[OH|AsO_4]$. Neu Jb Mineral, Mh 1971: 560–564

Kennedy CA, Stancescu M, Marriott RA, White MA (2007) Recommendations for accurate heat capacity measurements using a Quantum Design physical property measurement system. Cryogenics 47: 107–112

Koděra M (ed) (1990) Topographic Mineralogy of Slovakia. Veda, Bratislava, pp 1–1590 (in Slovak)

Krivovichev SV, Zolotarev AA, Popova VI (2016) Hydrogen bonding and structural complexity in the $Cu_5(PO_4)_2(OH)_4$ polymorphs (pseudomalachite, ludjibaite, reichenbachite): combined experimental and theoretical study. Struct Chem 27: 1715–1723

Krivovichev SV, Hawthorne FC, Williams PA (2017) Structural complexity and crystallization: the Ostwald sequence of phases in the $Cu_2(OH)_3Cl$ system (botallackite–atacamite–clinoatacamite). Struct Chem 28: 153–159

Magalhães MCF, De Jesus JDP, Williams PA (1988) The chemistry of formation of some secondary arsenate minerals of Cu(II), Zn(II) and Pb(II). Mineral Mag 52: 679–690

Majzlan J (2017) Solution calorimetry on minerals related to acid mine drainage – methodology, checks, and balances. Acta Geol Slov 9: 171–183

Majzlan J, Lang BE, Stevens R, Navrotsky A, Woodfield BF, Boerio-Goates J (2003) Thermodynamics of iron oxides: Part I. Standard entropy and heat capacity of goethite (α-FeOOH), lepidocrocite (γ-FeOOH), and maghemite (γ-Fe_2O_3). Amer Miner 88: 846–854

Majzlan J, Zittlau A, Grevel K-D, Schliesser J, Woodfield BF, Dachs E, Števko M, Chovan M, Plášil J, Sejkora J, Milovská S (2015) Thermodynamic properties and phase equilibria of the secondary copper minerals libethenite, olivenite, pseudomalachite, kröhnkite, cyanochroite, and devilline. Canad Mineral 53: 937–960

Majzlan J, Števko M, Dachs E, Benisek A, Plášil J, Sejkora J (2017) Thermodynamics, stability, crystal structure, and phase relations among euchroite, $Cu_2(AsO_4)(OH)\cdot 3H_2O$, and related minerals. Eur J Mineral 29: 5–16

Mincheva-Stefanova I (1968) Strashimirite, a new hydrous copper arsenate. Zap Vsesojuz Mineral Obsh 97: 470–477

Mindat. Accessed on February 1, 2022 at https://www.mindat.org/min-3799.html

Navrotsky A, Mazeina L, Majzlan J (2008) Size-driven structural and thermodynamic complexity in iron oxides. Science 319: 1635–1638

Nordstrom DK, Munoz JL (1994) Geochemical Thermodynamics, 2nd edition. Blackwell Scientific, Boston, pp 1–493

Nordstrom DK, Königsberger E, Majzlan J (2014) Thermodynamic properties for arsenic minerals and aqueous species. In: Bowell RJ, Alpers CN, Jamieson HE, Nordstrom DK, Majzlan J (eds) Arsenic: Environmental Geochemistry, Mineralogy, and Microbiology. Mineralogical Society of America and Geochemical Society Reviews in Mineralogy and Geochemistry 79: 217–255

Ondruš P, Veselovský F, Hloušek J, Skála R, Vavřín I, Frýda J, Čejka J, Gabašová A (1997) Secondary minerals of the Jáchymov (Joachimsthal) ore district. J Czech Geol Soc 42: 3–69

Parker VB (1965) Thermal properties of uni-univalent electrolytes. National Stand Ref Data Series, Natl Bur Stand 2: pp 1–66

Perchiazzi N, Demitri N, Fehér B, Vignola P (2017) On the crystal-chemistry of rosasite and parádsasvárite. Canad Mineral 55: 1027–1040

Petříček V, Dušek M, Palatinus L (2014) Crystallographic computing system JANA2006: general features. Z Kristall 5: 345–352

Petříček V, Dušek M, Palatinus L (2020) Crystallographic computing system JANA2020. Institute of Physics, Czech Academy of Sciences, Prague

Piret P, Deliens M (1988) Description de la ludjibaïte, un polymorphe de la pseudomalachite, $Cu_5(PO_4)_2(OH)_4$. Bull Minéral 111: 167–171

Plumhoff A (2021) Thermodynamic Properties, Crystal Structures, Phase Relations and Isotopic Studies of Selected Copper Oxysalts. Unpublished PhD thesis, Friedrich Schiller University, Jena, pp 1–118

Pouchou JL, Pichoir F (1985) "PAP" (φρZ) procedure for improved quantitative microanalysis. In: Armstrong JT (ed) Microbeam Analysis. San Francisco Press, pp 104–106

Robie RA, Hemingway BS (1995) Thermodynamic properties of minerals and related substances at 298.15 K and 1 bar (10^5 Pascals) pressure and at higher temperatures. U.S. Geol Surv Bull 2131: 1–461

Rumsey M, Welch M, Spratt J, Kleppe A, Števko M (2021) Kernowite, $Cu_2Fe(AsO_4)(OH)_4\cdot 4H_2O$, the Fe^{3+}-analogue of liroconite from Cornwall, UK. Mineral Mag 85: 283–290

Sejkora J, Bureš B (2020) Copper arsenates from the ore stope at the Geschieber vein – north (Daniel level), Svornost, the Jáchymov ore district (Czech Republic). Bull Mineral Petrol 28: 454–465 (in Czech)

Sejkora J, Plášil J, Ondruš P, Veselovský F, Císařová I, Hloušek J (2010) Slavkovite, $Cu_{13}(AsO_4)(AsO_3OH)_4\cdot 23H_2O$, a new mineral species from Horní Slavkov and Jáchymov, Czech Republic: description and crystal-structure determination. Canad Mineral 48: 1157–1170

Sejkora J, Plášil J, Veselovský F, Císařová I, Hloušek J (2011) Ondrušite, $CaCu_4(AsO_4)_2(AsO_3OH)_2\cdot 10H_2O$, a new mineral species from the Jáchymov ore district, Czech Republic: description and crystal-structure determination. Canad Mineral 49: 885–897

Sejkora J, Škácha P, Dvořák Z, Muzikant P (2015) Slavkovite from Preisselberg, the Krupka ore district (Czech Republic) and its mineral association. Bull mineral-petrol odd Nár Muz (Praha) 23: 1–18 (in Czech)

Sheldrick GM (2015) SHELXT – integrated space-group and crystal-structure determination. Acta Crystall A 71: 3–8

Shoemaker GL, Anderson JB, Kostiner E (1981) The crystal structure of a third polymorph of $Cu_5(PO_4)_2(OH)_4$. Amer Miner 66: 169–175

Sieber NHW, Tillmanns E, Medenbach O (1987) Hentschelite, $CuFe_2(PO_4)_2(OH)_2$, a new member of the lazulite group, and reichenbachite, $Cu_5(PO_4)_2(OH)_4$, a polymorph of pseudomalachite, two new copper phosphate minerals from Reichenbach, Germany. Amer Miner 72: 404–408

Southwood M, Števko M, Carr P (2020) Tsumeb: zincolivenite and the adamite–olivenite series. Rocks Miner 95: 210–232

Tost F (2021) Syntheses im Kupferphosphat–Arsenat-System. Unpublished MSci. thesis, Friedrich Schiller University, Jena, pp 1–65

Weiland T (2013) Die bedeutendsten Fundstellen für Kupfermineralien. In: Kupfer Mineralien. ExtraLapis 45: 30